On the long-term context of the 1997–2009 'Big Dry' in South-Eastern Australia: insights from a 206-year multi-proxy rainfall reconstruction

Joëlle Gergis · Ailie Jane Eyre Gallant · Karl Braganza · David John Karoly · Kathryn Allen · Louise Cullen · Rosanne D'Arrigo · Ian Goodwin · Pauline Grierson · Shayne McGregor

Abstract This study presents the first multi-proxy reconstruction of rainfall variability from the mid-latitude region of south-eastern Australia (SEA). A skilful rainfall reconstruction for the 1783–1988 period was possible using twelve annually-resolved palaeoclimate records from the Australasian region. An innovative Monte Carlo calibration and verification technique is introduced to provide the robust uncertainty estimates needed for reliable climate reconstructions. Our ensemble median reconstruction captures 33% of inter-annual and 72% of decadal variations in instrumental SEA rainfall observations. We investigate the stability of regional SEA rainfall with large-scale circulation associated with El Niño–Southern Oscillation (ENSO) and the Inter-decadal Pacific Oscillation (IPO) over

J. Gergis (✉) · A. J. E. Gallant · D. J. Karoly
School of Earth Sciences, University of Melbourne, Melbourne, VIC 3010, Australia
e-mail: jgergis@unimelb.edu.au

K. Braganza
Australian Bureau of Meteorology, GPO Box 1289, Melbourne, VIC 3001, Australia

K. Allen
School of Biological Sciences, Monash University, Melbourne, VIC 3800, Australia

L. Cullen · P. Grierson
School of Plant Biology, University of Western Australia, Perth, WA 6907, Australia

R. D'Arrigo
Tree-ring Laboratory, Lamont Doherty Earth Observatory, Palisades, NY 10964, USA

I. Goodwin
Department of Environmental and Geography, Macquarie University, Sydney, NSW 2109, Australia

S. McGregor
Climate Change Research Centre, University of New South Wales, Sydney, NSW 2052, Australia

the past 206 years. We find evidence for a robust relationship with high SEA rainfall, ENSO and the IPO over the 1840–1988 period. These relationships break down in the late 18th–early 19th century, coinciding with a known period of equatorial Pacific Sea Surface Temperature (SST) cooling during one of the most severe periods of the Little Ice Age. In comparison to a markedly wetter late 18th/early 19th century containing 75% of sustained wet years, 70% of all reconstructed sustained dry years in SEA occur during the 20th century. In the context of the rainfall estimates introduced here, there is a 97.1% probability that the decadal rainfall anomaly recorded during the 1998–2008 'Big Dry' is the worst experienced since the first European settlement of Australia.

1 Introduction

During 1997–2009, south-eastern Australia (SEA) was in the grip of the 'Big Dry'. Severe short-term rainfall deficiencies occurred in late 1997, 2002, 2006 and 2008, and were accompanied by a notable absence of intervening wet years. SEA has also experienced systematic reductions of 10–20% in autumn and early winter rainfall, which have resulted in unprecedented accumulated rainfall deficits (Timbal et al. 2010). Until the very strong 2010–2011 La Niña event eased some of the ongoing rainfall deficits in SEA, the prolonged drought affected water availability, agriculture and ecosystem functioning in a region that supports approximately 60% of Australia's population and around 40% of the nation's total agricultural production (Hennessy et al. 2007).

Given that gridded rainfall observations are only available from 1900 onward, considerable uncertainty about the range and nature of decadal-scale rainfall variability still exists (Power et al. 1999a). Determining how much of this 13-year drought was caused by natural, decadal-scale variability and/or anthropogenic climate change projected for the mid-latitudes of the globe, is now a major research priority. Recent research shows that the rainfall deficiencies recorded between 1997–2009 were the worst in Australia's instrumental record, with modelling studies suggesting a link to the strengthening of the sub-tropical ridge associated with global warming (Timbal et al. 2010). Average surface temperatures over Australia have increased by 0.7°C since 1960, while maximum day-time temperatures have risen by nearly 1°C in SEA over the past 50 years (Timbal et al. 2010). The nature of observed rainfall deficits in SEA suggests that recent changes are related to natural drought variability compounded by positive trends in temperature and pressure consistent with increased greenhouse gases (Timbal et al. 2010).

This study uses the Australian Bureau of Meteorology's definition of SEA by the area east of 135°E and south of 33°S, including Tasmania (http://www.bom.gov.au/climate/change/about/temp_timeseries.shtml) (Fig. 1). The region's rainfall is influenced by seasonally-dependent, tropical–extra-tropical interactions in the Pacific, Indian and Southern Oceans (Murphy and Timbal 2008; Risbey et al. 2009). Assessing the key drivers of Australian rainfall variability, Risbey et al. (2009) concluded that ENSO is the leading driver of Australian rainfall variability in terms of overall spatial coverage and consistency through all seasons. Specifically, the SEA region receives most of its rainfall during the winter half of the year, at a time when the Australian rainfall–ENSO relationship is most significant (Murphy and Timbal 2008; Risbey et al. 2009). Overall, ENSO accounts for approximately 20–25% of the total annual rainfall variance in SEA (Murphy and Timbal 2008; Risbey et al. 2009).

There is a need to assess the long-term stability of regional teleconnection patterns associated with large-scale global circulation features like the El Niño–Southern Oscillation
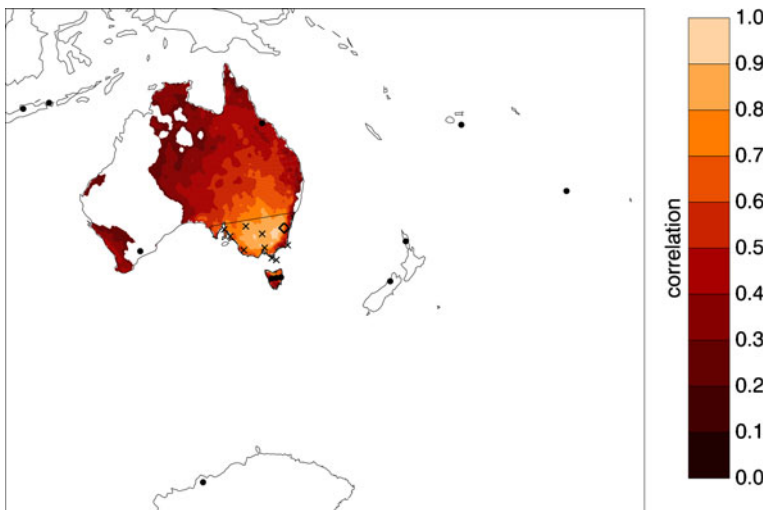
Fig. 1 Correlations between annual variations in May–April southeast Australia area-averaged rainfall and point rainfall on the Australian continent. The boundary of southeast Australia as defined in this study is outlined in black. The locations of the proxy data (*solid circles*), the high-quality station data (*crosses*) and the location of Lake George (*open diamond*) are shown

(ENSO) that drive contemporary rainfall variations in the region. For example, three of the last four La Niña events (1998–1999, 1999–2000, 2007–2009), which have historically delivered good rain to south-eastern Australia (SEA), failed to bring drought relief to the region (Murphy and Timbal 2008; Gallant and Karoly 2009). Furthermore, the influence of ENSO on Australian rainfall has been shown to be asymmetrical (Power et al. 1998; Power et al. 2006), spatially complex (Wang and Hendon 2007; Taschetto and England 2008) and known to vary over time (Hendy et al. 2003; Power et al. 2006). Although the strength of La Niña, measured through either central Pacific SSTs or the Southern Oscillation Index (SOI), is a good indication of the magnitude of positive rainfall anomalies, the strength of an El Niño is not the best guide to the severity of rainfall deficiencies (Power et al. 2006). There is also recent evidence to suggest that ENSO is itself varying in response to global warming (Power and Smith 2007).

On decadal timescales, there is a significant relationship between increased Australian rainfall and the negative phase of the Inter-decadal Pacific Oscillation (Power et al. 1999a, b). During positive (negative) IPO phases, correlations between the ENSO and Australian climate weaken and the Pacific enters a more El Niño (La Niña)-like state (Power et al. 1999a, b). Power et al. (1999b) found that the variance of the SOI is over twice as large during negative IPO phases compared to the SOI variance during positive IPO conditions. To date, decadal variability in Australian climate has only been subject to a handful of instrumental records, modelling and palaeoclimate studies (Power et al. 1999a; Hendy et al. 2003; Power and Colman 2006; Lough 2007). A recent instrumental study by Ummenhofer et al. (2011) reports that on decadal timescales, variations in SEA rainfall are more strongly correlated to Indian Ocean sea surface temperatures than Pacific Ocean conditions.

Palaeoclimate reconstructions offer a unique way of examining decadal regional climate variability in the pre-industrial period, allowing us to interpret recently observed rainfall variations under different low frequency mean-state conditions experienced outside of the

instrumental period. A recent pilot reconstruction of broad-scale monsoon drought variability in the Australasian region showed that considerable reconstruction skill – up to 40% of the inter-annual variance in the September–January Palmer Drought Severity Index (PDSI) for the 0°–40°S, 95°–155°E region – could be achieved using as few as three well-dated annually-resolved palaeoclimate records (D'Arrigo et al. 2008). The authors concluded that there was much potential to improve regional drought reconstructions using more proxy records from Australasia.

The aim of the current study is to provide extended estimates of rainfall variations for the SEA region using an expanded proxy network, placing the 1997–2009 'Big Dry' into a long-term context. As only three local composite tree ring records are available from directly within SEA, we take a somewhat experimental approach to reconstructing regional rainfall variability by predominately using remote proxies from the Australasian region. We use an observational data network to demonstrate that records from locations with established teleconnection relationships between SEA rainfall and the Pacific, Indian and Southern Oceans can be used to reconstruct regional rainfall variability, bearing important caveats in mind. The first is that any reconstruction of SEA rainfall based on a remote proxy network can only capture a portion of the total variability related to the large-scale drivers of regional rainfall; principally, ENSO, the Indian Ocean Dipole (IOD) and the Southern Annular Mode (SAM) (Risbey et al. 2009). Variance associated with local atmospheric circulation operating on seasonal scales is unlikely to be captured by a network of remote proxies, thus cannot be reflected in the imperfect rainfall estimates presented here. Nonetheless, our reconstruction remains valuable since drought in the region is heavily influenced by the decadal-scale variability in rainfall (Power et al. 1999a), which is dominated by large-scale circulation associated with ENSO, IOD and SAM (Risbey et al. 2009; Timbal et al. 2010; Ummenhofer et al. 2011).

Recently, there have been concerted efforts to improve the quantification of uncertainty in past climate reconstructions (National Academy of Sciences 2006; Burger 2007; Li et al. 2007). Over-fitting palaeoclimate reconstructions to 20th century observations during the calibration process, which has the effect of underestimating the prediction error, may result in unrealistic reconstructions (Braganza et al. 2009). This is associated with, but not confined to, inadequately estimating uncertainty resulting from (i) the assumption of linear statistical relationships between proxies and a given climate variable, and (ii) the 'stationarity' assumption that the statistical relationship between a proxy and a given climate variable remains stable during the calibration, verification and reconstructed period (National Academy of Sciences 2006).

To improve the uncertainty estimates of our rainfall reconstruction, we introduce an 'ensemble' technique using Monte Carlo resampling for calibration and verification to provide a histogram (rather than single measure) of reconstruction uncertainty. We use a network of annually-resolved palaeoclimatic records from the Australasian region to provide a reconstruction of past rainfall variations in south-eastern Australia (SEA) for the A.D. 1783–1988 period. Principal Component Analysis (PCA) is used to develop a multi-proxy, area-averaged rainfall reconstruction with robust uncertainty estimates for the SEA region. We investigate the ability of the proxy network to predict SEA rainfall variability associated with high and low frequency ENSO, the main driver of SEA rainfall. Finally we examine apparent fluctuations in decadal-scale wet and dry phases in SEA rainfall and IPO variability over the past two centuries, and assess the 'Big Dry' in the context of decadal variability captured by our new 206-year rainfall reconstruction.

2 Data and methods

2.1 Instrumental data

Rainfall data were obtained from the Australian Bureau of Meteorology for calibration and verification of the palaeoclimate reconstruction. Monthly Australian Water Availability Project (AWAP) data were available from January 1900 to April 2009 on a 0.05°×0.05° surface across Australia (Jones et al. 2009). The monthly rainfall surfaces were interpolated using data from at least 3000 rainfall gauges located around Australia (Jones et al. 2009). Annual rainfall totals were converted to anomalies relative to the period of overlap between the proxy and instrumental data (1900–1988), before being area-averaged over the SEA region. For comparison with the proxy data, the area-averaged SEA time series was then normalised by subtracting by the mean and dividing by the standard deviation over the 1900–1988 period. Annual rainfall was averaged over a May–April year as this period has the strongest association between SEA rainfall variations and ENSO (Risbey et al. 2009) and variations in the palaeo network (detailed in section 2.2).

In addition, a subset of nine precipitation records from well-spaced stations across SEA (Table 1) was examined to extend the observed rainfall record back to 1873. These rainfall records have been checked for length, completeness and inhomogeneities and are referred to as 'high quality' records by the Australian Bureau of Meteorology (Lavery et al. 1997; Trewin and Fawcett 2009). The data were area-weighted over SEA using Thiessen polygons (Thiessen 1911). The high-quality subset captured over 86% of the variance in the gridded SEA rainfall data over the period 1900–2005, indicating that a few, well-placed stations are able to capture spatially-coherent rainfall variations in SEA.

To examine the influence of ENSO on SEA rainfall reconstructions over the 1900–1988 period, we use the Troup (1965) Southern Oscillation Index (SOI) accessed from the Bureau of Meteorology (http://www.bom.gov.au/climate/current/soihtm1.shtml), a coupled atmosphere–ocean index (CEI) of Gergis and Fowler (2005) and the Niño 3.4 Sea Surface Temperature (SST) index (Trenberth and Stepaniak 2001). To consider the influence of non-Pacific Ocean variations on the region, we use the Dipole Mode Index (Saji et al. 1999) and an index of the Southern Annular Mode (Marshall 2003) for the 1900–1988 and 1957–1988 periods, respectively. Finally, we analyse relationships with the Inter-decadal Pacific Oscillation (IPO) (Power et al. 1999a) to investigate low frequency variability components of SEA rainfall and multi-year wet and dry conditions. Here, decadal-scale Pacific

Table 1 Nine monthly high quality rainfall stations used from 1873–1988 to examine SEA annual rainfall to extend the Australian Bureau of Meteorology's gridded AWAP network

Station number	Latitude	Longitude	Station name
22020	33.93°S	137.63°E	Wallaroo
23721	35.06°S	138.56°E	Happy Valley Reservoir
26025	37.38°S	140.84°E	Penola Post Office
47053	34.11°S	141.91°E	Wentworth Post Office
74128	35.55°S	144.95°E	Deniliquin Post Office
84016	37.57°S	149.91°E	Gabo Island Lighthouse
86131	37.56°S	145.13°E	Yan Yean
85096	39.13°S	146.42°E	Wilsons Promontory Lighthouse
99001	39.48°S	147.32°E	Deal Island

variability is represented by the unfiltered monthly IPO anomaly normalised to a 1911–1995 base period (http://www.iges.org/c20c/IPO_v2.doc) averaged over a May–April year and smoothed with an 11-year running mean.

Ideally, reconstructions of regional climate variability are based upon proxy climate indicators from the local region, however this is not always possible. To date, no suitable long, annually-resolved proxy records have been developed or published for the SEA region aside from the Tasmanian tree ring records listed in Table 2. Instead we exploit the fact that large-scale weather and climate drivers influence a great deal of inter-annual and decadal rainfall variability in SEA. That is, we attempt to reconstruct rainfall variability in SEA using proxies representing ENSO variability and other broad-scale climate modes.

The 'pseudo proxy' analysis presented in supplementary S1 shows that modern climate observations derived from Global Historical Climatology Network (GHCN) stations (Peterson and Vose 1997) in close proximity to each of the proxy record locations (Table 2 and Fig. 1), can be used to skilfully predict regional rainfall in SEA. All records show sensitivity to local climate and/or regional scale circulation features in the southeast Australian region. Using established teleconnection relationships between SEA rainfall and the Pacific, Indian and Southern Oceans, we show that a network of twelve climate stations can successfully capture up to 85% of SEA rainfall variance related to Pacific and non-Pacific variability on decadal timescales (see supplementary material S1 and S2).

2.2 Palaeoclimate reconstruction method

We perform Principal Component Analysis (PCA) analysis (Jolliffe 2002) on the twelve palaeoclimate records listed in Table 2 (processed as outlined in supplementary S3) to

Table 2 Australasian palaeoclimate data used in this study, A.D. 1783–1988. All proxy variables are calendar year dated with the exception of the Great Barrier Reef 'master' coral chronology (October–September year) and the Law Dome ice core (May–July average)

Proxy data	Dates	Location	Proxy variable	Reference/s
Huon Pine tree-rings	1600 BC −1989	SE Australia	Total ring width	Cook et al. (2000)
Western Australia *Callitris* tree-rings	1655–2005	SW Australia	Total ring width	Cullen and Grierson (2009)
Celery Pine tree-rings (western Tasmania)	1290–1998	SE Australia	Total ring width	Allen et al. (2001); Allen (2002); La Marche et al. (1979)
Celery Pine tree-rings (eastern Tasmania)	1152–1994	SE Australia	Total ring width	Allen et al. (2001); Allen (2002); La Marche et al. (1979)
Kauri tree-rings	1724 BC–2002	New Zealand	Total ring width	Fowler et al. (2008)
Pink Pine	1450–1999	New Zealand	Total ring width	Fenwick (2003); Duncan et al. (2010)
Teak tree-rings	1565–2000	Indonesia	Total ring width	D'Arrigo et al. (2006)
Rarotonga coral	1727–1996	SW Pacific	Sr/Ca	Linsley et al. (2000)
Bali corals	1782–1989	SW Pacific	δO18	Charles et al. (2003)
Great Barrier Reef corals	1631–1983	NE Australia	Luminescence (Oct–Sep)	Lough (2007)
Fiji–Tonga corals	1650–2001	SW Pacific	δO18 (four core average)	Linsley et al. (2008)
Law Dome ice-core	1300–1995	Antarctica	Na (May–Jul)	Goodwin et al. (2004)

extract the common temporal modes of variability from the proxy network. Figure 1 shows that these palaeoclimate records are mostly remote from SEA with the exception of Tasmanian tree ring records. Although rainfall in Tasmania shows weaker correlations compared with locations on mainland Australia, unfortunately there are currently no suitable annually-resolved palaeoclimate records in the study region on the mainland. For this initial analysis, the time interval common to all records was analysed (1783–1988), to avoid issues associated with the declining number of proxies available further back in time. All proxies and instrumental data were normalised relative to the common period of overlap (1900–1988) prior to the generation of the reconstruction and then rescaled to represent rainfall anomalies in millimetres for the final reconstruction.

The correlations between the time series of the first PC, representing the largest amount of common variance (Table 3), with area-averaged SEA rainfall were calculated for all possible 3, 6, 9 and 12-month periods. Although there were several periods that contain strong correlations with palaeo PC1, we selected the 12-month period from May–April to capture the common response of the palaeo network and ENSO in the instrumental record. To remove extraneous noise that was not associated with SEA rainfall variations, only the PCs that showed a statistically significant correlation (at 5%, two-tailed significance according to a Student's t-test) with annual rainfall for at least 20% of the SEA region were

Table 3 Eigenvector loadings for individual proxies and PCs 1–3 of the palaeoclimate network. Pearson correlations between PC1, PC2 and PC3 times series and (i) south-eastern Australian rainfall, (ii) Southern Oscillation Index (SOI), (iii) Niño 3.4 SSTs, (iv) Coupled ENSO Index (CEI), (v) Dipole Mode Index (DMI) and (vi) Southern Annular Mode (SAM). All indices were averaged over a May–April year for the 1900–1988 period, except for the SAM index that is only available from 1957 onward. Bolded values are significant to 0.05 level and italicised correlations are not statistically significant. All other correlations are correlations significant to 0.01 level

| Proxy data	PC1	PC2	PC3
New Zealand Kauri tree-rings	0.19	−0.19	−0.15
New Zealand Pink Pine tree rings	−0.01	−0.06	−0.15
Indonesian Teak tree-rings	0.35	0.14	−0.37
Western Australian Callitris tree-rings	−0.13	−0.08	−0.25
Tasmanian Huon Pine tree-rings	0.44	−0.26	−0.09
Western Tasmania Celery Pine tree-rings	0.17	0.16	−0.29
Eastern Tasmania Celery Pine tree-rings	−0.17	0.79	−0.14
Fiji–Tonga coral	−0.32	−0.47	−0.27
Great Barrier Reef corals	−0.46	−0.23	0.01
Rarotonga coral	0.31	0.01	0.82
Bali corals	−0.55	0	−0.06
Law Dome ice-core	−0.02	−0.05	−0.11
Variance (%)	17	12	12
Climate indices			
SEA rainfall	−0.40	−0.34	−0.30
SOI	−0.48	**−0.27**	−0.36
Niño 3.4 SSTs	−0.47	*−0.20*	−0.33
CEI	−0.51	**−0.22**	−0.36
DMI	**0.24**	*0.17*	0.17
SAM	*−0.16*	*0.16*	*0.03*

selected. Using this technique, PCs 1–3 were selected for subsequent analysis, together representing 41% of the covariance in the proxy network. The raw PC time series and the statistically significant correlations between PCs 1–3 and instrumental May–April SEA rainfall for the 1900–1988 period are shown in Fig. 2.

Using multiple, ordinary least squares linear regression, PCs 1–3 were regressed against observed area-average SEA annual rainfall data to develop the SEA annual rainfall reconstruction. In this way, the original twelve proxy records were reduced to three independent potential predictors of SEA rainfall. All three modes contributed approximately evenly to the median reconstruction regression model coefficients (PC1: $\beta=-0.17$, $2\sigma=0.07$, PC2: $\beta=-0.20$, $2\sigma=0.10$ and PC3: $\beta=-0.20$, $2\sigma=0.11$). Multiple reconstructions were developed using an innovative Monte Carlo resampling technique to produce an ensemble of reconstructions. The method uses 10,000 random selections of five independent decades of sequential ten-year blocks between 1900 and 1988, with each sample determining the parameters for the multiple regression model for that reconstruction. The remaining years were used for verification against the 20th century observations using metrics described below. The use of independent decades of data goes someway to preserving decadal climatic variations, which are large in SEA rainfall. Errors between each ensemble member and the instrumental data followed a normal distribution and had low autocorrelations that were similar to those of the instrumental rainfall record (see supplementary S4). The decadal reconstructions were calculated by smoothing the annual reconstructions (i.e. each ensemble member) using an 11-year centred moving average. The decadal error estimates were recomputed from these smoothed reconstructions.

We use a suite of calibration and verification metrics (Cook and Kairiukstis 1990) to estimate the uncertainty (i.e. unresolved variance) associated with various calibration intervals on inter-annual and decadal timescales. The following verification statistics were calculated: r is the Pearson correlation coefficient; ar^2 is square of the multiple correlation coefficient following adjustment for loss of degrees of freedom; RE is reduction of error statistic and RMSE is root mean square error (Cook and Kairiukstis 1990). CE is the coefficient of efficiency statistic and is more rigorous than RE as it uses independent data (i.e. the verification period) for its calculation (Cook and Kairiukstis 1990). Note that RE and CE values greater than zero indicate model skill and there is no significance level per se (Cook and Kairiukstis 1990). The sign test (ST) described by Fritts (1976) indicates how accurately the regression model tracks observed inter-annual and inter-decadal climate anomalies. The statistical significance of the correlation coefficients have been determined independently for annual and decadal data, so as to account for the loss of degrees of freedom in the decadal data.

The final 'best estimate' rainfall reconstruction is the median of the 10,000-member ensemble. The confidence interval was calculated as two standard deviations of the error distribution either side of the median reconstruction. These uncertainty bounds combined the errors representing random or 'climate' noise and the spread of the ensemble members generated from the random selection of calibration periods, described as the 'calibration error'. By using multiple, randomly selected calibration periods, the potential that the data will be over-fitted to one period from the instrumental record is reduced. As Australian

Fig. 2 The correlations between annual May–April rainfall and the first three principal components determined from the twelve proxy records calculated over the 1900–1988 period. Statistically significant correlations only (determined using Student's T-test) are shown. Red (blue) contours denote positive (negative) correlations. The solid black line indicates the boundary of the SEA study region. The time series of each raw PC are also given
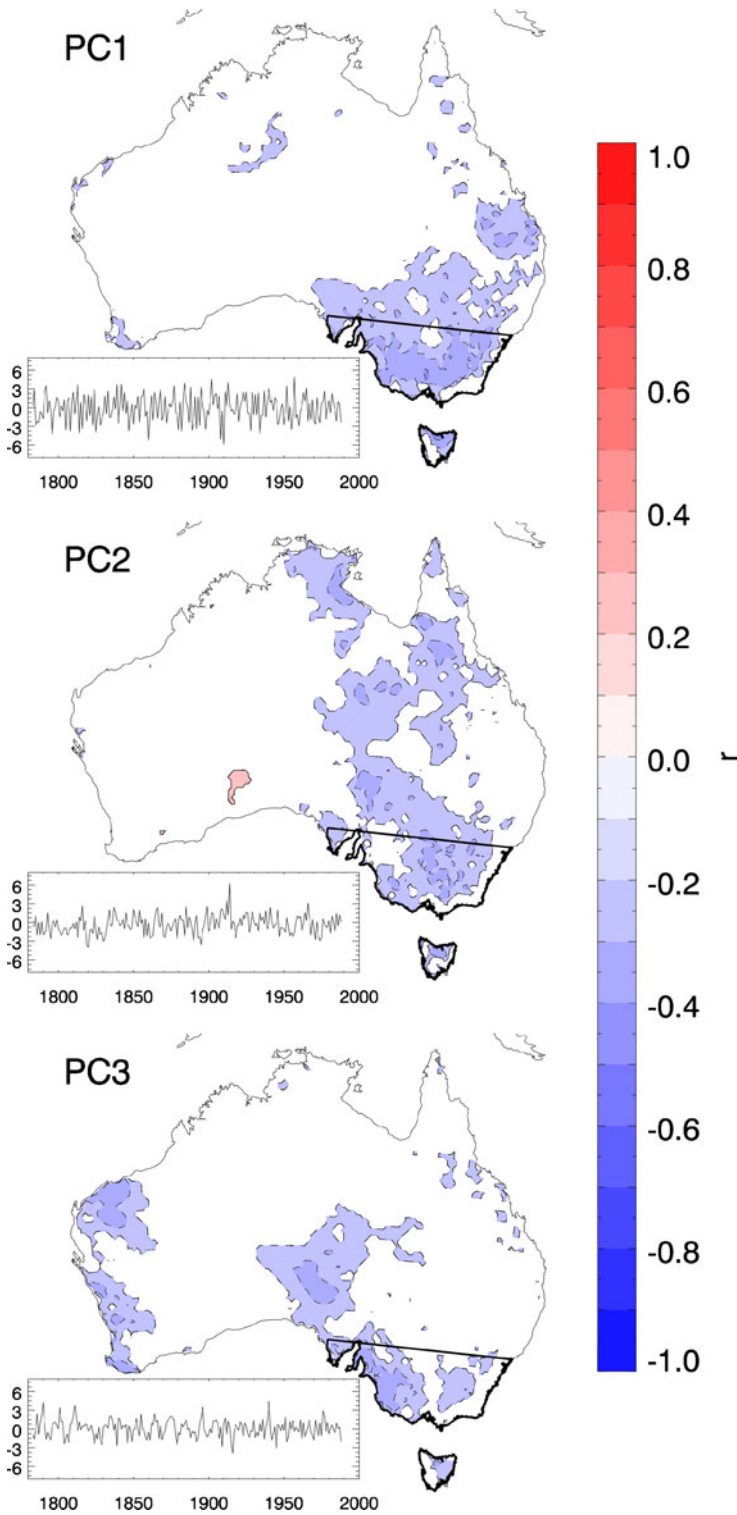
rainfall is highly variable, the approach also ensures that calibration biases or biases in the apparent skill of the model during the verification period are represented in the error estimates (the 'calibration error' described above). In addition to the 10,000 verification tests run using 20th century, instrumental rainfall data from an additional subset of nine stations from the Bureau of Meteorology's high quality rainfall network (Table 1) within SEA were area-averaged and also examined over the 1873–1988 period (see supplementary S5).

3 Results

3.1 Reconstruction calibration and verification

Model skill was first assessed using conventional 'split calibration' techniques routinely used by palaeoclimatologists (Cook and Kairiukstis 1990), where half of the data were withheld for verification or the full period of overlap was used for calibration. The statistics calculated using early 20th century, late 20th century or the full period of overlap varied considerably, demonstrating that model skill was sensitive to the selected calibration interval (Table 4). For example, for the annual data, the late 20th century (1945–1988) calibration produced poor model skill within the verification period (1900–1944). However, when early 20th century calibration was performed, the model verified robustly. This indicates that arbitrary selection of a single period for calibration and verification may not adequately represent the best estimate of model skill.

To specifically address this issue of calibration sensitivity, we developed a Monte Carlo resampling technique to produce a suite of reconstructions based on randomly selecting 10,000 calibration/verification combinations over the 1900–1988 period (described in section 2.2). So instead of a single measure of reconstruction skill, we present an empirical probability histogram of the verification statistics calculated from each of the 10,000 reconstructions resampled over the 1900–1988 period on inter-annual and decadal timescales (see Table 5 and supplementary S4). As described in section 2.2, we use 50 (39) years for calibration (verification) over the 1900–1988 period.

The correlation coefficient between the instrumental record and the reconstruction ensemble median for the calibration period on inter-annual timescales was 0.57,

Table 4 Comparison of calibration and verification sensitivity using a) full period calibration (1900–1988), b) early period calibration (1900–1944) c) late period calibration (1945–1988) and d) the median of the Monte Carlo ensemble. All statistics are the same metrics presented in Table 5

Statistic	a) Full period calibration (1900–1988)	b) Early period calibration (1900–1944)	c) Late period calibration (1945–1988)	d) Monte Carlo calibration median (1900–1988)
$r_{calibration}$	0.57	0.41	0.71	0.57
ar^2	0.30	0.11	0.46	0.33
$r_{verification}$	–	0.70	0.41	0.55
RE	–	0.39	0.16	0.13
CE	–	0.27	−0.02	0.10
ST	–	(35/45) 78%	(24/20) 56%	(27/12) 69%
RMSE	–	0.85	0.98	0.94

Table 5 Inter-annual a) calibration and b) verification statistics were calculated for each of the 10,000 reconstructions using random selections of 50 years of data between 1900 and 1988. The results are presented as the median statistic from the reconstruction ensemble (the reconstruction statistics are normally distributed) with uncertainty estimates given as ± two standard deviations. The following statistics were calculated: r is the Pearson correlation coefficient; ar^2 is square of the multiple correlation coefficient following adjustment for loss of degrees of freedom; RE is reduction of error statistic and RMSE is root mean square error and CE is the coefficient of efficiency statistic. Decadal c) calibration and d) verification statistics as described above using the gridded AWAP rainfall observations (1900–1988). Decadal e) calibration and f) verification statistics as described above using the nine rainfall stations in Table 1 (1873–1988)

a) 1900–1988 inter-annual calibration		b) 1900–1988 inter-annual verification					
r	ar^2	r	RE	CE	ST		RMSE
0.57±0.08	0.33±0.09	0.55±0.10	0.13±0.21	0.10±0.21	27/12 ±2/2 (69%±5%)		0.94±0.08
c) 1900–1988 decadal calibration		d) 1900–1988 decadal verification					
r	ar^2	r	RE	CE	ST		RMSE
0.85±0.15	0.70±0.25	0.85±0.19	0.73±0.32	0.66±0.52	27/6±8/6 (80%±20%)		0.56±0.19
e) 1873–1988 decadal calibration		f) 1873–1988 decadal verification					
r	ar^2	r	RE	CE	ST		RMSE
0.68±0.34	0.40±0.40	0.63±0.27	0.35±0.26	0.26±0.17	43/15±10/10 (73%±17%		0.85±0.13

representing approximately 33% of inter-annual variability of the observed rainfall record. The distribution of annual rainfall is effectively an independent Gaussian distribution and so the statistical significance of this relationship was measured by the t-test. The agreement between the observations and the reconstruction is statistically significant (two-tailed) at the below the 0.01% level. Although the median RE and CE statistics shown in Table 5 are only modestly positive for the median reconstruction, 74% (67%) of the reconstructions returned positive RE (CE) statistics, indicating model skill in tracking inter-annual variations beyond the mean of the verification (calibration) period. The sign test results for the median reconstruction returned a 27/12 ratio of agreements/disagreements with the calibration period observations indicating that the agreement in the sign of the inter-annual variations in the reconstruction with rainfall observations is greater than random chance (significant at the 0.01 confidence level). An experiment using instrumental climate data from the same locations suggests that this could be improved to almost 50% (see supplementary S1), perhaps with further refinements/combinations of the palaeo network, and will be the subject of future work.

On decadal timescales, the skill of the reconstruction during the 20th century calibration and verification intervals rises dramatically, reflected in the positive RE result in all but 0.4% of ensemble members (Table 5). The correlation coefficient between the instrumental data and the ensemble median for the calibration period is 0.85, capturing approximately 72% of decadal variations in observed SEA rainfall, or approximately 40% more variance than the annual time series. The inflation of the decadal correlation may be associated with smoothing of time series, where the introduction of temporal dependence can lead to stronger correlations. Therefore, to determine the statistical significance of this association, the loss of the degrees of freedom associated with smoothing must be taken into account. Statistical significance effectively determines the chance that two unrelated time series will produce the observed correlation. So, producing 10,000 pairs of independent synthetic annual rainfall series, smoothing these in the same way as the reconstructions and correlating the two, tested statistical significance for the decadal reconstruction. From these simulations, we found that the correlation of 0.85 in the decadal time series was statistically significant at below the 0.01% level (two-tailed). Hereafter, the significance levels for the

correlations computed using decadally-smoothed time series are computed in the above manner, to account for the loss of the degrees of freedom associated with smoothing. The strong ability of the palaeo network to reproduce variations in 20th century SEA decadal rainfall is also apparent in the histograms of each metric, representing the distribution of all possible values (see supplementary S4).

The results are weaker when calibrating using the 1873 subset of nine rainfall stations (Table 5), which captures approximately 46% of observed decadal rainfall variance. The statistical agreement between the palaeoclimate data and the 1873 rainfall subset may reflect the fact that none of the long rainfall stations (Table 1) come from Tasmania, where many of the tree ring records from the region are located (Table 2). Although there is good agreement between the reconstructions calibrated using the 1873 subset and AWAP data (supplementary S5), the stronger AWAP calibration/verification results presented in Table 5 led to us relinquishing the longer calibration length provided by the 1873 subset in favour of the AWAP observations, which includes between 2853–7278 stations across a wider area of the SEA region.

As mentioned previously, palaeoclimate reconstructions should not be expected to reproduce the full range of observed climate variability with complete fidelity. It is clear that the SEA rainfall reconstruction has most skill on decadal rather than inter-annual timescales and that this skill is statistically significant. That is, our reconstruction is most skilful in capturing decadal-scale variability associated with the large-scale circulation modes of ENSO, SAM and the IOD, providing valuable estimates of the magnitude of 'boundary' decadal variability for SEA.

3.2 Climate sensitivity of the proxy network

Table 6 shows that on inter-annual timescales, SEA rainfall shows a maximum correlation of $r=0.56$ with the SOI (significant at the 0.01 level). Correlations are also significant with the DMI ($r=-0.33$), suggesting Pacific and Indian Ocean variability are the dominant influences on SEA rainfall variability in the May–April annual year period. While there is debate surrounding the independence of Indian Ocean variations from Pacific Ocean variability and its role in SEA droughts (Ummenhofer et al. 2009; Smith and Timbal 2010), the western Indian Ocean SST variations have long been recognised as important modulators of Australian rainfall (Nicholls 1989) so the results for the commonly cited DMI are presented here for ease of comparison. Statistically insignificant relationships with the SAM are probably reflective of the region chosen for SEA, and the fact that the SAM influences rainfall in the winter half of the year in coastal areas south of the Great Dividing Range (Hendon et al. 2007). On decadal timescales, a correlation of $r=-0.77$ with the IPO and SEA decadal rainfall is observed. Taking into account the loss of degrees of freedom as described previously, this relationship is statistically significant at the 0.02% level.

Having assessed the relative influence of the main drivers of SEA rainfall variations, correlations were then calculated between the gridded instrumental May–April Australian inter-annual rainfall and the three leading palaeo principal components derived from the PC analysis. Figure 2 shows statistically significant associations (at the 0.05 level), indicating that the palaeo network has a clear association with rainfall variations throughout much of the SEA region. Table 3 shows the correlations between palaeo PCs 1–3 with SEA rainfall and ENSO, DMI and SAM indices. On inter-annual timescales, the correlation between palaeo PC1 and SEA rainfall is $r=-0.40$ and the maximum correlation with an ENSO index is −0.51 with the Coupled ENSO Index (both significant at the 0.01 level). These results closely match the strength of the correlations seen between observed ENSO indices and SEA rainfall in the 1900–1988 period (Table 6). There is no discernable

Table 6 Pearson correlations of AWAP area-averaged SEA rainfall data and the SEA rainfall reconstruction with (i) Southern Oscillation Index (SOI), (ii) Niño 3.4 SSTs, (iii) Coupled ENSO Index (CEI), iv) Dipole Mode Index (DMI), (v) Southern Annular Mode (SAM) and (vi) Inter-decadal Pacific Oscillation (IPO). All indices were averaged over a May–April year for the 1900–1988 period, except for the SAM index that is only available from 1957 onward. Note that decadal correlations were only calculated between observed and reconstructed SEA rainfall and the low frequency IPO index, not inter-annual climate modes. All correlations (except SAM) are significant to 0.05 or 0.01 level

Climate indices (May–April average)	SEA rainfall observations	SEA rainfall reconstruction
Inter-annual (1900–1988)		
SEA rainfall	–	0.57
SOI	0.56	0.63
Niño 3.4 SSTs	0.49	0.56
CEI	0.52	0.62
DMI	−0.33	−0.32
SAM (1957–1988 only)	0.10	−0.01
Decadal (1905–1983)		
SEA rainfall	–	0.85
IPO	−0.77	−0.64

geographical pattern in the eigenvector loadings of PCs 1–3 for individual proxy records, indicating that there is no single location that heavily weights the reconstruction. This suggests that the palaeo network reflects the diverse circulation features influencing SEA.

On decadal timescales, our rainfall reconstruction shows a strong ability to reproduce observed changes in SEA rainfall, and its interactions with low frequency ENSO variability (Table 6). We find strong, statistically significant associations between 11-year running averages of our SEA rainfall reconstruction, and observed rainfall and the IPO. Correlations between our rainfall reconstruction and the May–April IPO instrumental index over the period 1900–1988 are high ($r=-0.64$, significant at the 0.1% level) and reflect a similar relationship between the instrumental SEA rainfall and IPO time series ($r=-0.77$, significant at the 0.02% level) (Table 6).

Although there is skill in the inter-annual results, the remainder of this paper focuses on our conservative decadal rainfall reconstruction calibrated using the AWAP observational rainfall data over the 1900–1988 period to provide long-term assessment of the protracted 1997–2009 drought.

3.3 Decadal wet and dry phases of the SEA rainfall reconstruction

To investigate broad-scale decadal variations in SEA rainfall, next we examine multi-year wet and dry phases over the 1788–1988 period. Here we define sustained wet or dry phases as negative or positive anomalies greater ±0.5 standard deviations or more, lasting three years or longer in the 11-year smoothed reconstruction and rainfall observations (Fig. 3b). The rainfall observations display the following prolonged wet and dry periods: 1936–1945 (dry), 1949–1960 (wet), 1968–1976 (wet), 1980–1982 (dry), 1988–1991 (wet) and 1997–2002 (dry). There is very good agreement between the observed wet and dry phases and the reconstructed protracted events (Table 7). There is, however, a tendency for the reconstruction to slightly overestimate the length of these intervals as recorded in the instrumental period, perhaps indicative of a greater low frequency (biological) responses in the proxies compared to the rainfall observations.

Fig. 3 The SEA rainfall reconstruction from 1783–1988 at **a** inter-annual and **b** decadal time-scales. The solid black line represents the median of the distribution of 10,000 rainfall reconstructions. The grey shading indicates ± two standard deviations of the error distribution, calculated as the combined errors between the reconstruction ensemble members and the observations associated with the calibration period and the random errors associated with 'climate noise'. The dashed line shows the instrumental AWAP rainfall data used for 20th century calibration and verification (1900–1988)
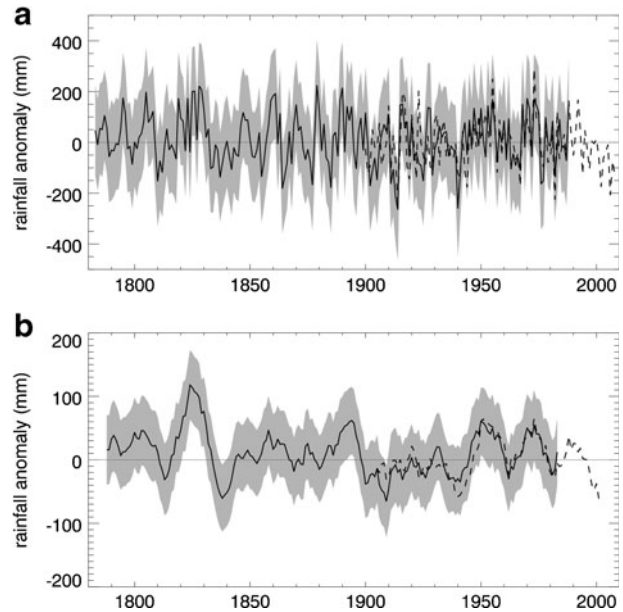
One noticeable feature in the reconstruction is the duration of wet intervals experienced during the late 18th/early 19th century (e.g. the 13-year period from 1797–1809 and 16-year wet phase from 1818–1833). This compares with a 12-year pluvial (1949–1960) seen in the 20th century instrumental record. The longest dry spells recorded in the reconstruction are eight years from 1835–1842 and from 1935–1942. The longest drought seen in the rainfall observations during the 1905–1988 period is the ten-year interval spanning 1936–1945. In comparison to a markedly wetter late 18th/early 19th century containing 75% of sustained wet years, 70% of all reconstructed sustained dry year periods in SEA occur during the 20th century. No prolonged wet period has been observed in the reconstruction since 1976 and since 1991 in the instrumental rainfall record (at the time of writing)

Table 7 Wet and dry phases greater than ±0.5 standard deviation lasting three years or more in the 11-year filtered south-eastern Australian rainfall reconstruction, 1788–1983. Negative and positive IPO phases derived from an 11-year smoothed version of McGregor et al.'s (2010) inter-annual Unified ENSO Proxy (UEP) reconstruction are also shown

SEA wet periods	IPO negative phases	SEA dry periods	IPO positive phases
1788–1793	–	–	1788–1799
1797–1809	1800–1823	1812–1815	–
1818–1833		1835–1842	1824–1854
1856–1865	1855–1870	1900–1904	1899–1918
1887–1897	1874–1898	1906–1911	
–	1919–1925	1914–1918	
1946–1959	1946–1960	1924–1927	1926–1945
1969–1976	1965–1971	1935–1942	–
–	–	–	1961–1964

3.4 How unusual was the 1998–2008 'Big Dry'?

The historical context of the most recent drought in south-eastern Australia is currently the subject of much discussion. Recent research suggests that the duration and magnitude of the 1997–2009 rainfall anomaly is now the largest recorded in SEA in the historical record dating back to 1900; 45% worse than the previous 1933–1945 drought record (Timbal et al. 2010). To provide a long-term perspective on this issue, we now address the question: how unusual is the 'Big Dry' in the context of the past two centuries?

To assess where the recent drought lies in the distribution of natural decadal variability captured by our rainfall estimates, we compared the minimum 11-year mean rainfall anomaly in instrumental record (i.e. the decade 1998–2008), with all the decadal rainfall anomalies generated from the 10,000-member rainfall reconstruction back to 1788 and AWAP rainfall observations (1900–2009) (Fig. 4). The solid vertical line in Fig. 4 indicates the position of the 1998–2008 rainfall anomaly in relation to the entire distribution of the reconstruction ensemble. From this, we calculated that there is only a 2.9% probability that a dry decade exceeding the 1998–2008 anomaly has been experienced over the 1783–2008 period. Bearing in mind the uncertainty and caveats associated with the rainfall estimates presented here, the result suggests that there is a 97.1% chance that the 1998–2008 'Big Dry' is the worst drought experienced since European settlement of Australia.

Recall that the annual reconstruction was scaled to have the same variance as the observations during the period of overlap. However, smoothing meant that the variance of the decadal reconstruction and observations were not necessarily the same. This difference might affect the probabilistic estimate of the 'Big Dry' rainfall deficit occurring during the last 206 years. To examine this sensitivity, we extracted the ensemble members that had comparable variance to the observations only, where comparable was defined as differences in the variance of less than 5%. The use of this subset made little difference to the result, changing the probability to 2.8%.

It should also be noted that this assessment of the current prolonged drought is limited to meteorological drought (rainfall deficits) and does not take into account factors like surface temperature that influence the severity of hydrological drought. Similarly, the reconstruction does not account for seasonal affects noted previously. In particular, the depth of the drought in autumn and early winter has been identified as unique in the instrumental record (Timbal et al. 2010).

Fig. 4 Histogram of all 11-year mean rainfall anomalies generated from the 10,000-member rainfall reconstruction (1783–1988) and AWAP rainfall observations (1900–2009). The solid vertical line indicates the 1998–2008 decadal rainfall anomaly in relation to the full reconstruction ensemble
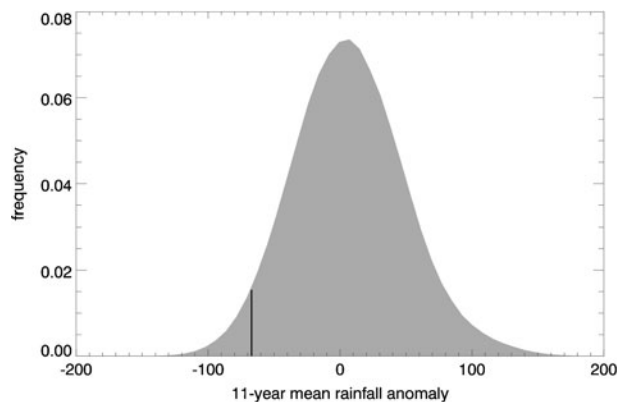
3.5 Stability of the SEA rainfall–ENSO teleconnection relationship

To assess the long-term stability of the SEA rainfall–ENSO teleconnection we now compare our ensemble median rainfall reconstruction with the Unified ENSO Proxy (UEP) developed by McGregor et al. (2010). The UEP represents the first uncalibrated EOF of ten published ENSO reconstructions back to A.D. 1650 and a decadally-smoothed version has been used as a proxy of the IPO (see McGregor et al. (2010) for further details). Since a number of the palaeoclimate records used in our previous ENSO reconstructions (Braganza et al. 2009) are used in the current study, the UEP was recalculated removing the Braganza et al. (2009) data (proxies three and nine in McGregor et al. (2010)) to provide independent comparison with the SEA rainfall reconstruction introduced here. As discussed in the McGregor et al. (2010) paper, the UEP is not reliant on any single proxy reconstruction so it is no surprise that the UEP (minus the Braganza et al. 2009 data) compares very well with original UEP (correlation coefficient of 0.97).

Figure 5a shows the relationship between 11-year running averages of our SEA rainfall and the UEP (inverted and lagged by one year) over the 1788–1971 period of overlap. The UEP is lagged by one year to synchronise the growing season of the Australasian tree-ring records (which straddle two calendar years over the austral summer), with the same calendar year of the eastern Pacific tree ring dominated reconstructions. Figure 5b shows the relationship of 21-year running correlation between the inter-annual SEA rainfall reconstruction and the UEP (again excluding Braganza et al. (2009)). McGregor et al.'s (2010) work suggests five sustained positive IPO phases and six negative IPO phases over the 1788–1971 period (Table 7).

Although a correlation of $r = -0.46$ (two-tailed significance at the 6% level) is found for the inter-annual variations over the full period of overlap, it is clear from 21-year running
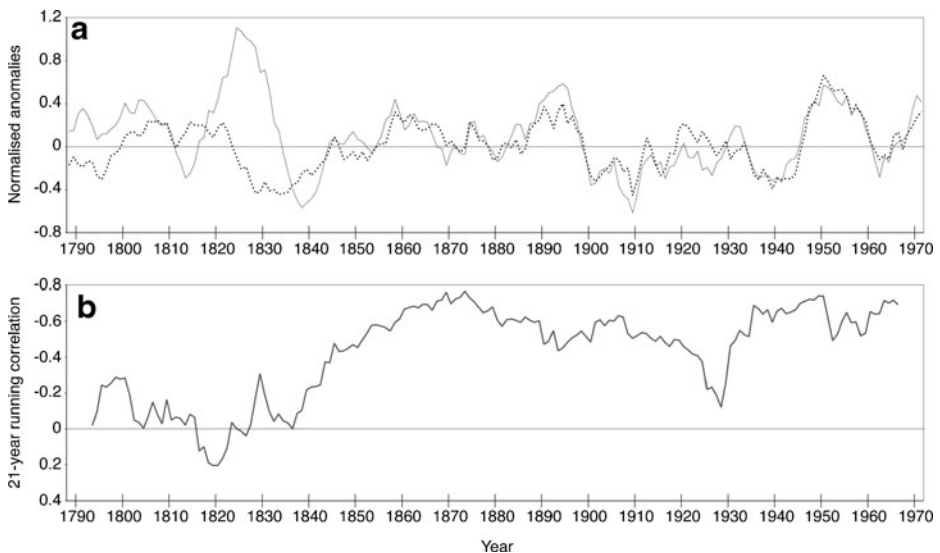

Fig. 5 a 11-year running means of the SEA rainfall reconstruction (the ensemble median, shown by the solid line) and the Unified ENSO Proxy (dashed line) from 1788–1971. Note that the UEP has been inverted and lagged by one year for comparison with the SEA rainfall reconstruction and anomalies are relative to a common 1900–1976 base period. b 21-year running correlation of the inter-annual variations of the SEA rainfall reconstruction and the UEP, 1793–1966. Note that the y-axis has been inverted

correlations between the two inter-annual time series that there is a marked breakdown of the relationship around the year 1839 (Fig. 5b). From 1840 onwards, the inter-annual (decadal) correlation is $r=0.58$ ($r=0.86$), which is significant at the 0.01% level in both cases. The correlation between the decadal rainfall reconstruction and the IPO during the 1788–1839 period is 0.01. Possible explanations for this apparent breakdown are presented in the discussion. We also identify the well-recognised 20th century weakening of the ENSO–SEA rainfall relationship centred on 1930 discussed previously in the literature (Power et al. 1998). The most notable breakdown in the strength of the low frequency ENSO/IPO variability and SEA rainfall relationship in our reconstruction is observed in the pre-1840s period (Fig. 5b). Intriguingly, this period is associated with sustained positive rainfall anomalies despite the presence of positive IPO conditions.

4 Discussion

Unfortunately, the ideal scenario of using multiple, annually-resolved proxy records from within SEA as local predictors of SEA rainfall is not possible due to only three composite tree ring records from directly within the study region. As an alternative, we have selected a range of records from a broader Australasian region that encompass the key large-scale circulation features that influence SEA. Using established teleconnection relationships between SEA rainfall and climate variability in the Pacific, Indian and Southern Oceans, we show that, remarkably, a predominately remote network of just twelve climate stations can successfully capture up to 85% of decadal SEA rainfall variations (see supplementary S1 and S2).

The above results, however, must be interpreted with important caveats borne in mind. The first is that any reconstruction of regional SEA rainfall based on a remote proxy network can only capture the fraction of total variability related to the large-scale circulation features like ENSO. Variance associated with localised dynamical features operating on seasonal scales cannot be completely represented by a network of remote proxies, and consequently the 'imperfect' rainfall reconstruction presented here. Nevertheless, our rainfall estimates are still valuable since drought in SEA is heavily influenced by the decadal-scale variability associated with large-scale circulation associated with ENSO, IOD and SAM (Risbey et al. 2009; Timbal et al. 2010; Ummenhofer et al. 2011). Since the low frequency component of SEA rainfall represents a significant fraction of the total variability, the reconstruction provides a robust estimation of likely prolonged wet and dry periods in the pre-instrumental period, that may be partly attenuated by unresolved, localised inter-annual variability.

The reconstruction is able to skilfully reproduce rainfall variations approximately the same proportion of variation explained by Indo–Pacific variability (see Table 6). The sensitivity of the SEA rainfall reconstruction to Pacific and Indian Ocean SSTs variations is also expected given the fact that many of the proxy records used in this study come from western Pacific locations strongly influenced by ENSO. However the analysis presented in supplementary S2 shows that our proxy network is responding to both Pacific and non-Pacific climate variability on decadal timescales, indicating the reconstruction captures more than just ENSO variability. In particular the Indian Ocean proxies listed in Table 3 are strongly loaded in PC1 that is consistent with the Indian Ocean being strongly related to SEA rainfall variability on decadal timescales (Ummenhofer et al. 2011).

It is possible that the non-coherence of low frequency ENSO and SEA rainfall experienced during the 1788–1839 period is due to dating errors in the palaeoclimate records. However, this is unlikely as single proxy records with known dating errors

(Dunbar et al. 1994) or fragmentation issues over our target period (Cobb et al. 2003) are not used in this study or have zero or low eigenvector loadings in the UEP analysis (McGregor et al. 2010). To test the sensitivity of the result to potential dating uncertainties, we removed all the coral records from the SEA rainfall reconstruction to just contain the well-replicated tree ring records (and one ice core) to see if the breakdown in the apparent SEA rainfall–ENSO relationship might be due to dating errors associated with less-replicated proxy records. However, the marked decline remains, suggesting that the feature is unlikely to be caused by palaeoclimate dating uncertainties.

To further test the stability of individual proxy–ENSO relationships we briefly analysed the 21-year running correlations of the individual proxies in Table 3 with the UEP (not shown). All records show either a weakening (e.g. New Zealand Kauri), marked decline (e.g. Indonesian Teak,) weakening or sign reversal (e.g. Fiji–Tonga coral) in their correlation with ENSO conditions during the pre-1840 period. Finally, the very nature of PCA extracts dominant modes of covariability, so it is unlikely that the twelve proxy records used in this analysis all have synchronous dating errors.

As such, we are inclined to believe that the feature may represent a true decoupling of SEA rainfall from ENSO during the 1783–1840 period. Despite the positive IPO phase condition in the 1783–1799 period, the SEA rainfall reconstruction indicates predominately wet conditions spanning the 1783–1833 (with a brief dry interval from 1812–1815). Figure 5 suggests that the IPO–SEA rainfall relationship has not remained stable through time, and may indicate alternative forcing of regional climate variability during this period, such as a greater influence of the extra-tropical longwave trough associated with SAM variability (Goodwin et al. 2004) or some association between enhanced tropical volcanism noted during this period (D'Arrigo et al. 2009).

To investigate the likelihood that the reconstructed wet phase centred on the 1820s (Fig. 3b) is indeed real and not an artifact of our methodology or proxy data issues, we consulted an historical lake level record for the inland Lake George reported from 1817–1918 (Russell 1877). Lake George is a precipitation-sensitive basin in New South Wales with no known outlet and strong correlations to SEA rainfall (see Fig. 1). It has long been recognised as having highly variable lake levels due to its location west of the Great Dividing Range, a mountain chain that provides an orographic barrier to easterly rain-bearing systems reaching inland Australia (Russell 1877). As such, fluctuations in its water level reflect regional rainfall variability over time, providing us with an extremely useful independent rainfall proxy located directly in the SEA study region.

According to historical sources, two 'chief maxima' in Lake George levels occurred around 1821 and in 1875 (C.E.P.B 1923). Russell (1877) reports that the lake contained water between 1817 and 1828, and perhaps achieved its highest level in June 1823. For example in 1821 the lake was described as a 'magnificent sheet of water' and in 1824 was reported to be '20 miles long and 8 miles wide, almost entirely enclosed with thickly-wooded, steep hills'. Declining lake levels are reported from 1832, culminating in the severe drought around 1840 (Russell 1877), also seen in Fig. 3b. The agreement of fluctuations in Lake George levels and the SEA rainfall reconstruction confirms the likelihood that the marked wet phase in our reconstruction is indeed a real feature of regional climate variations experienced during the early 19th century.

While the SEA rainfall ENSO/IPO relationship is robust over the mid 19th to late 20th century, the evidence presented here suggests that factors influencing rainfall variability during the 1788–1840 period in the SEA region are not associated with ENSO or the IPO, which are the dominant drivers of inter-annual and decadal-scale rainfall variability in the contemporary climate record. There are various possible causes for these changes in the

relationship between ENSO and SEA rainfall around the mid-1800s shown in Fig. 5. They are, that the changes represent: (i) changes in the location of ENSO's centre of action; (ii) switched dominance of regional climate drivers, and (iii) changes in solar and/or volcanic forcing (Mann et al. 2000; D'Arrigo et al. 2009; McGregor et al. 2010). Although the period of increased SEA rainfall and the apparent breakdown in the SEA–ENSO relationship coincides with reduced global temperatures associated with the Little Ice Age, cooling of tropical SSTs and volcanism (D'Arrigo et al. 2009), no causal mechanism is proposed here as no model comparisons are presented.

Clearly there is a need for high quality climate reconstructions from the Australasian region to complement the Northern Hemisphere palaeoclimate detection and attribution studies (Mann et al. 2005; Hegerl et al. 2006, 2007). As multi-proxy palaeoclimate reconstructions are reduced to the 'lowest common denominator' resolution, collectively they are unable to resolve monthly–seasonal variability consistently throughout the year. They do, however, offer the possibility of examining anomalies accumulated on inter-annual–decadal timescales, and as such, are helpful in extending estimates of natural variability inadequately captured by instrumental records. In this way, palaeoclimate estimates of past rainfall and temperature variations from the Australian region could be used to better-isolate natural decadal-scale variability, offering a powerful way of constraining regional climate change projections.

5 Conclusions

This study presents the first multi proxy rainfall reconstruction for the mid-latitude region of south-eastern Australia for the 1783–1988 period. Significantly, we estimate that there is a 97.1% probability that the decadal rainfall anomaly recorded during the 'Big Dry' is the worst since first European settlement in Australia. The Monte Carlo ensemble calibration and verification technique presented here provides robust uncertainty estimates based on the probability histogram of a suite of 10,000 rainfall reconstructions. This method attempts to account for sensitivities in model skill to the traditional single period calibration/verification intervals routinely applied in palaeoclimate studies. This will allow reconstruction skill to be stringently assessed in the next IPCC assessment and supports the case for further work on ensemble approaches to multi proxy analysis (Li et al. 2007; van der Schrier et al. 2007; Neukom et al. 2010; Gallant and Gergis 2011).

The strong SEA rainfall–ENSO relationship has been robust over the 1840–1988 period and corresponds closely with fluctuations in the IPO. The apparent pre-1840 decoupling of SEA rainfall variability from ENSO/IPO forcing reported here confirms the need for further extensions of our reconstruction to examine the nature and stability of the ENSO teleconnection in SEA over longer time scales. From the results introduced here, it is clear that the 1998–2008 'Big Dry' is unusual in the context of the past two centuries. Further work is now needed to extend estimates of natural climate variability in the south east Australian region to provide a firmer basis for the detection and attribution of mid-latitude anthropogenic climate change and the study of past Australian societies' responses to climate variability since 1788.

References

Allen KJ (2002) The temperature response in the ring widths of *Phyllocladus Aspleniifolius* (celery-top pine) along an altitudinal gradient in the Warra LTER Area, Tasmania. Aust Geogr Stud 40(3):287–299

Allen KJ, Cook E, Francey R, Michael K (2001) The climatic response of *Phyllocladus aspleniifolius* (Labill.) Hook. f in Tasmania. J Biogeogr 28:305–316

Braganza K, Gergis J, Power S, Risbey J, Fowler A (2009) A multiproxy index of the El Nino–Southern Oscillation, A.D. 1525–1982. J Geophys Res 114(D5):D05106

Burger G (2007) On the verification of climate reconstructions. Clim Past 3:397–409

C.E.P.B (1923) Variations in the level of Lake George, Australia. Nature 112(2825):918

Charles C, Cobb K, Moore M, Fairbanks R (2003) Monsoon–tropical ocean interaction in a network of coral records spanning the 20th century. Mar Geol 201(1–3):207–222

Cobb K, Charles C, Cheng H, Edwards L (2003) El Nino/Southern Oscillation and tropical Pacific climate during the last millennium. Nature 424:271–276

Cook E, Kairiukstis L (1990) Methods of dendrochronology. Kluwer Academic Publishers, Dordrecht

Cook E, Buckley B, D'Arrigo R, Peterson M (2000) Warm-season temperatures since 1600 BC reconstructed from Tasmanian tree rings and their relationship to large-scale sea surface temperature anomalies. Clim Dyn 16:79–91

Cullen L, Grierson P (2009) Multi-decadal scale variability in autumn-winter rainfall in south-western Australia since 1655 AD as reconstructed from tree rings of Callitris columellaris. Clim Dyn 33(2–3):433–444

D'Arrigo R, Wilson R, Palmer J, Krusic P, Curtis A, Sakulich J, Bijaksana S, Zulaikah S, Ngkoimani L, Tudhope A (2006) The reconstructed Indonesian warm pool sea surface temperatures from tree rings and corals: Linkages to Asian monsoon drought and El Nino–Southern Oscillation. Paleoceanography 21 (PA3005):PA3005/1–PA3005/13

D'Arrigo R, Baker P, Palmer J, Anchukaitis K, Cook G (2008) Experimental reconstruction of monsoon drought variability for Australasia using tree rings and corals. Geophys Res Lett 35:L12709. doi:10.1029/2008GL034393p1-6

D'Arrigo R, Wilson R, Tudhope A (2009) The impact of volcanic forcing on tropical temperatures during the past four centuries. Nat Geosci 2:51–56

Dunbar R, Wellington G, Colgan M, Glynn P (1994) Eastern Pacific sea surface temperature since 1600 AD: the d18O record of climate variability in Galapagos corals. Paleoceanography 9:291–316

Duncan RP, Fenwick P, Palmer JG, McGlone MS, Turney CSM (2010) Non-uniform interhemispheric temperature trends over the past 550 years. Clim Dyn 35(7–8):1429–1438

Fenwick P (2003) Reconstruction of past climates using pink pine (Halocarpus biformus) tree-ring chronologies. Christchurch, New Zealand, Soil Plant and Ecological Sciences, Linclon University

Fowler A, Boswijk G, Gergis J, Lorrey A (2008) ENSO history recorded in *Agathis australis* (Kauri) tree-rings Part A: Kauri's potential as an ENSO proxy. Int J Climatol 28(1):1–20

Fritts H (1976) Tree rings and climate. Academic Press Inc., London

Gallant AJE, Gergis J (2011) An experimental streamflow reconstruction for the River Murray, Australia, 1783–1988. Water Resour Res 47:W00G04: doi:10.1029/2010WR009832

Gallant AJE, Karoly DJ (2009) Atypical influence of the 2007 La Niña on rainfall and temperature in southeastern Australia. Geophys Res Lett 36(L14707): doi:10.1029/2009GL039026

Gergis J, Fowler A (2005) Classification of synchronous oceanic and atmospheric El Niño-Southern Oscillation (ENSO) events for palaeoclimate reconstruction. Int J Climatol 25:1541–1565

Goodwin I, van Ommen T, Curran M, Mayeweski P (2004) Mid latitude winter climate variability in the South Indian and southwest Pacific regions since 1300 AD. Clim Dyn 22:783–794

Hegerl GC, Crowley TJ, Hyde WT, Frame DJ (2006) Climate sensitivity constrained by temperature reconstructions over the past seven centuries. Nature 440(7087):1029–1032

Hegerl GC, Crowley TJ, Allen M, Hyde WT, Pollack HN, Smerdon J, Zorita E (2007) Detection of human influence on a new, validated 1500-year temperature reconstruction. J Clim 20(4):650–666

Hendon H, Thompson D, Wheeler M (2007) Australian rainfall and surface temperature variations associated with the Southern Hemisphere Annular Mode. J Clim 20:2452–2465

Hendy E, Gagan M, Lough J (2003) Chronological control of coral records using luminescent lines and evidence for non-stationary ENSO teleconnections in northeastern Australia. Holocene 13(2):187–199

Hennessy K, Fitzharris B, Bates B, Harvey N, Howden S, Hughes L, Salinger J, Warrick R (2007) Australia and New Zealand. Climate Change 2007: impacts, adaptation and vulnerability. Contribution of Working Group II to the Fourth Assessment Report of the Intergovernmental Panel on Climate Change. Cambridge University Press, Cambridge, pp 507–540

Jolliffe IT (2002) Principal component analysis, 2nd edn. SpringerVerlag, New York

Jones DA, Wang W, Fawcett R (2009) High-quality spatial climate data-sets for Australia. Aust Meteorol Oceanogrc J 58:233–248

La Marche V, Holmes J, Dunwiddie P, Drew G (1979) Tree-ring chronologies of the Southern Hemisphere: 4. Australia. Laboratory of Tree-Ring Research, University of Arizona, Tucson, USA

Lavery B, Joung G, Nicholls N (1997) An extended high-quality historical rainfall data set for Australia. Aust Met Mag 46:27–38

Li B, Nychka D, Ammann C (2007) The 'hockey stick' and the 1990s: a statistical perspective on reconstructing hemispheric temperatures. Tellus 59A:591–598

Linsley B, Wellington G, Schrag D (2000) Decadal sea surface temperature variability in the subtropical South Pacific from 1726 to 1997 AD. Science 290:1145–1149

Linsley B, Zhang P, Kaplan A, Howe S, Wellington G (2008) Interdecadal-decadal climate variability from multicoral oxygen isotope records in the South Pacific Convergence Zone region since 1650 A.D. Paleoceanography 23:1–16

Lough J (2007) Tropical river flow and rainfall reconstructions from coral luminescence: Great Barrier Reef, Australia. Paleoceanography 22(PA2218): doi: 10.1029/2006PA001377

Mann M, Bradley R, Hughes M (2000) Long-term variability in the El Niño/Southern Oscillation and associated teleconnections. In: Diaz H, Markgraf V (eds) El Nino and the Southern Oscillation; multiscale variability and global and regional impacts. Cambridge University Press, Cambridge, pp 327–372

Mann M, Cane M, Zebiak S, Clement A (2005) Volcanic and solar forcing of the tropical pacific over the past 1000 years. J Clim 18:447–456

Marshall G (2003) Trends in the Southern Annular Mode from observations and reanalyses. J Clim 16 (24):4134–4143

McGregor S, Timmermann A, Timm O (2010) A unified proxy for ENSO and PDO variability since 1650. Clim Past 6:1–17

Murphy B, Timbal B (2008) A review of recent climate variability and climate change in southeastern Australia. Int J Climatol 28:859–879

National Academy of Sciences (2006) Surface temperature reconstructions for the last 2,000 years. The National Academies Press, Washington DC

Neukom R, Luterbacher J, Villalba R, Küttel M, Frank D, Jones PD, Grosjean M, Esper J, Lopez L, Wanner H (2010) Multi-centennial summer and winter precipitation variability in southern South America. Geophys Res Lett 37(L14708): 10.1029/2010GL043680

Nicholls N (1989) Sea surface temperature and Australian winter rainfall. J Clim 2:418–421

Peterson TC, Vose RS (1997) An overview of the global historical climatology network temperature database. Bull Am Meteorol Soc 78(12):2837–2849

Power S, Colman R (2006) Multi-year predictability in a coupled general circulation model. Clim Dyn 26(2–3):247–272

Power SB, Smith IN (2007) Weakening of the walker circulation and apparent dominance of El Nino both reach record levels, but has ENSO really changed? Geophys Res Lett 34(18): doi: 10.1029/2007GL030854

Power S, Tseitkin F, Torok S, Lavery B, Dahni R, McAvaney B (1998) Australian temperature, Australian rainfall and the Southern Oscialltion, 1910–1992: coherent variability and recent changes. Aust Meteorol Mag 47:85–101

Power S, Casey T, Folland C, Colman A, Mehta V (1999a) Inter-decadal modulation of the impact of ENSO on Australia. Clim Dyn 15:319–324

Power S, Tseitkin F, Mehta V, Lavery B, Torok S, Holbrook N (1999b) Decadal climate variability in Australia during the twentieth century. Int J Climatol 19:169–184

Power S, Haylock M, Colman R, Wang X (2006) The predictability of inter-decadal changes in ENSO activity and ENSO teleconnections. J Clim 19:4755–4771

Risbey JS, Pook MJ, McIntosh PC, Wheeler MC, Hendon HH (2009) On the remote drivers of rainfall variability in Australia. Mon Weather Rev 137:3233–3253

Russell HC (1877) Climate of New South Wales: descriptive, historical, and tabular. Charles Potter, Government Printer, Sydney

Saji N, Goswami G, Vinayachandran P, Yamagata T (1999) A dipole mode in the tropical Indian Ocean. Nature 401:360–363

Smith IN, Timbal B (2010) Links between tropical indices and southern Australian rainfall. Int J Climatol: doi: 10.1002/joc.2251

Taschetto A, England M (2008) El Nino Modoki impacts on Australian rainfall. J Climate 22:1–27

Thiessen AH (1911) Precipitation averages for large areas. Mon Weather Rev 39:1082–1084

Timbal B, Arblaster J, Braganza K, Fernandez E, Hendon H, Murphy B, Raupach M, Rakich C, Smith IKW, Wheeler M (2010) Understanding the anthropogenic nature of the observed rainfall decline across South

Eastern Australia. Centre for Australian Weather and Climate Research (CAWCR) Technical Report No. 026: pp 202

Trenberth K, Stepaniak D (2001) Indices of El Nino evolution. J Clim 14:1697–1701

Trewin B, Fawcett R (2009) Reconstructing historical rainfall averages for the Murray–Darling Basin. Bull Aust Meteorol Oceanogr Soc 22:159–164

Troup A (1965) The Southern oscillation. Q J Roy Meteorol Soc 91:490–506

Ummenhofer C, England M, McIntosh P, Meyers G, Pook M, Risbey J, Gupta A, Taschetto A (2009) What causes Australia's worst droughts? Geophys Res Lett 36(L04706): doi:10.1029/2008GL036801

Ummenhofer C, Gupta A, Briggs P, England MH, McIntosh P, Meyers G, Pook M, Raupach M, Risbey J (2011) Indian and Pacific Ocean influences on Southeast Australian drought and soil moisture. J Clim 24:1313–1336

van der Schrier G, Osborn T, Briffa K, Cook E (2007) Exploring an ensemble approach to estimating skill in multiproxy palaeoclimate reconstructions. Holocene 17(1):119–129

Wang G, Hendon H (2007) Sensitivity of Australian rainfall to inter-El Nino variations. J Clim 20:4211–4226